nature chemistry

Article

https://doi.org/10.1038/s41557-026-02098-6

Understanding low-pressure CO_2 insertion chemistry in epoxide–CO_2 copolymerization catalysis

Received: 30 May 2025

Accepted: 11 February 2026

Published online: 30 April 2026

Check for updates

Rosie Thorogood [1,2], Katharina H. S. Eisenhardt [1,2], Madeleine L. Smith[1] & Charlotte K. Williams [1]

Despite many CO_2 use strategies being reliant on fast and selective CO_2 insertion reactions into metal-alkoxide bonds, in-depth studies into this chemistry remain rare. Here the effect of CO_2 pressure on the CO_2 insertion chemistry is studied using epoxide–CO_2 copolymerizations. Five high-performance literature catalysts are investigated under systematically varied CO_2 pressures, revealing kinetic profiles indicative of CO_2 insertion equilibria. For each catalyst, two key parameters describing the CO_2 insertion chemistry are determined: the equilibrium constant, K_{eq}, and the saturation CO_2 pressure above which catalytic performance is maximized, $P_{threshold}$. Generalizable correlations between copolymerization activity, K_{eq} and $P_{threshold}$ are uncovered and used to predict performances for four further catalyst–monomer combinations. These correlations are a direct link between CO_2 insertion chemistry and process operating conditions, providing a mechanistic framework and testing protocols to accelerate future catalyst development. These results should help deliver efficient scalable CO_2 use technologies, operating with minimal energy.

The chemical industry remains dependent on unsustainable, fossil carbon sources[1–3]. To move towards a circular carbon economy, there is an urgent need to replace them with renewable carbon, for example from biomass or waste CO_2, and to ensure the lowest possible energy consumption[1–3]. Scalable CO_2 use technologies are, therefore, essential for the future chemical industry, but should operate under the lowest feasible pressure and deliver maximum rates[1,4–6]. To effectively transform CO_2 into valuable products, catalysis is vital[7–10]. CO_2 insertion into metal-alkoxide bonds (M–OR) is a common step across many catalytic transformations, for example CO_2 coupling with epoxides to form cyclic carbonates or polycarbonates or with alcohols to form dialkyl carbonates[8,10,11]. In nature, the metalloenzyme Rubisco catalyses atmospheric CO_2 transformation into 3-phosphoglycerate, involving CO_2 insertion into a transient Mg(II)ene-diolate (alkoxide) species[5,12]. Related CO_2 insertions into metal hydroxide or aqua bonds (M–OH or M–H_2O) are implicated in the industrial high pressure catalytic reverse water gas shift reaction[5]. These CO_2 insertion steps are often proposed to occur rapidly and to be pre-rate limiting, challenging their direct investigation[9,13,14]. Increasing the scale and efficiency of these CO_2 transformations requires better understanding of the kinetics and thermodynamics of CO_2 insertion into metal-alkoxide bonds[15].

Most previous investigations of CO_2 insertion chemistry have applied stoichiometric reactions with metal alkoxides and/or hydroxides[16,17]. For example, zinc hydroxide complexes were shown to react with CO_2 in chemical equilibria[18,19]. Whilst stoichiometric studies can be useful, caution should be applied in generalizing their findings to catalytic processes. Such CO_2 insertions relevant to utilization catalysis should be studied under real process operating conditions.

In this work, we target carbon dioxide and epoxide ring-opening copolymerization (ROCOP) using catalysts that produce perfectly alternating polycarbonates and maximize carbon dioxide uptake[20,21]. These catalytic cycles also involve metal-alkoxide intermediates that react with carbon dioxide to produce a metal-carbonate species; in this field it is desirable to identify carbon dioxide insertion chemistry

[1]Department of Chemistry, University of Oxford, Oxford, UK. [2]These authors contributed equally: Rosie Thorogood, Katharina H. S. Eisenhardt.
e-mail: charlotte.williams@chem.ox.ac.uk

https://doi.org/10.1038/s41557-026-02098-6

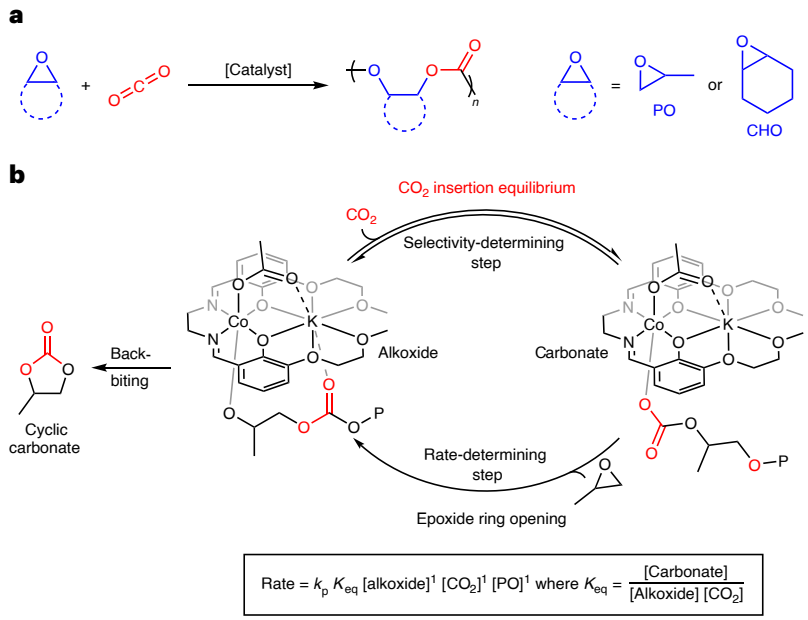

Fig. 1 | The ROCOP of epoxides and carbon dioxide. a, ROCOP of epoxides and CO_2 with the two most commonly studied epoxides: propene oxide (PO) and cyclohexene oxide (CHO). **b**, The proposed catalytic cycle for a high-performance Co(III)K(I) catalyst. The CO_2 insertion is proposed as an equilibrium and incorporated into the rate law[13].

that is effective at low catalyst (metal-alkoxide) concentrations and low CO_2 pressures. Previous kinetic and computational investigations, using a range of different catalysts, were generally conducted using higher carbon dioxide pressures (10–30 bar) and nearly always showed a zero order in CO_2 pressure; as a consequence, in this field catalysts were not designed or optimized for low CO_2 pressure insertion chemistry[13,14,22–25]. Very recently, we discovered the ROCOP of CO_2 and propene oxide (PO) using a heterodinuclear Co(III)K(I) catalyst, which showed good activity and selectivity at very low pressures. The catalyst also showed rates that depend on the CO_2 pressure applied over the range 2–12 bar. At higher pressures (12–30 bar), the rates are independent of pressure and are maximized[13]. Experimental kinetics and density functional theory calculations suggested that CO_2 insertion occurs by an equilibrium reaction between metal-alkoxide and metal-carbonate intermediates[13,14] (Fig. 1b). The CO_2 insertion equilibrium controls the effective concentration of the metal-carbonate intermediate, which is the catalytic species involved in the polymerization rate-determining step. Further, it influences catalyst selectivity, as the cyclic carbonate by-product forms from the metal alkoxide[13]. Before our work, only one other group reported two β-diiminate Zn(II) catalysts, used for cyclohexene oxide (CHO)–CO_2 ROCOP, that also showed pressure-dependent rates[26,27]. These previous reports, together with some suggestions of CO_2 pressure-dependent rates in other CO_2 insertion reactions[18,19,28], motivate the current in-depth investigation into how CO_2 pressure influences rates more generally in this field of copolymerization catalysis.

For industrially operable polymerizations, energy efficiency is important and this may be achieved by conducting reactions at moderate temperatures so as to balance rates, selectivity and polymer viscosity[29]. Further, reactions should be conducted at the lowest catalyst loadings feasible, particularly if residues must be removed before polymer use. In the past, there have been extensive investigations into the influences of catalyst loading and process temperature but much less understanding of how carbon dioxide pressure influences the catalysis[14,21,30,31]. Nonetheless, when copolymerization catalysts are effective at low carbon dioxide pressures ($P_{CO2} \leq 10$ bar), the resulting process financial costs (capex) and greenhouse gas emissions associated with gas compression are expected to be substantially lower[29]. To illustrate this point, Aspen Plus was used to estimate the changes to cost and energy input during poly(propene carbonate) (PPC) production due to CO_2 compression from 1 bar to 5 bar, 10 bar, 20 bar or 50 bar, respectively. These estimates suggest that increasing the CO_2 pressure from 5 bar to 20 bar, results in an increase of ~50% to the capital cost and >200% to the process energy requirement (Supplementary Table 1). These results highlight the economic and environmental benefits for lower pressure copolymerization catalysts.

Here the CO_2 insertion chemistry occurring during CO_2 and epoxide ROCOP catalysis is examined under industrially relevant process operating conditions, that is low catalyst loading (1:4,000 catalyst:epoxide), moderate temperature (50 °C) and minimized but fixed carbon dioxide pressure[9,20,32] (Fig. 1a). Epoxide–CO_2 ROCOP is an efficient CO_2 utilization process, forming useful polycarbonate products with high CO_2 uptakes, for example 43 wt% CO_2 in PPC[9,13,33–36]. These alternating polycarbonates are useful as surfactants, electrolytes and binders in batteries, thermoplastic elastomers, pressure sensitive adhesives and as engineering plastics[1,37–40]. To understand the influence of CO_2 pressure on copolymerization rates, we selected five known high-performance catalysts and investigated the influence of the carbon dioxide pressure applied to each of their polymerization rates. In all cases, the CO_2 pressure applied during the catalysis influences the copolymerization kinetics and for each catalyst the CO_2 insertion equilibrium constant is quantified. Combining the different catalyst threshold pressures and insertion equilibria, we reveal a general method to evaluate, optimize and compare new catalysts. For new catalysts it is possible using a single experiment to predict the lowest CO_2 pressure required to achieve maximum rates and selectivity.

Results and discussion

Catalyst selection

Direct comparisons between catalysts in this field is challenging as rates are reported under individually selected and/or optimized conditions. Analysis of the literature shows many require high CO_2 pressures and moderate temperatures, challenging the selection of catalysts operating at the low pressures and higher temperatures desirable for scale-up (Supplementary Fig. 1). To select catalysts suitable for in-depth kinetic investigations of CO_2 pressure dependence, we

https://doi.org/10.1038/s41557-026-02098-6

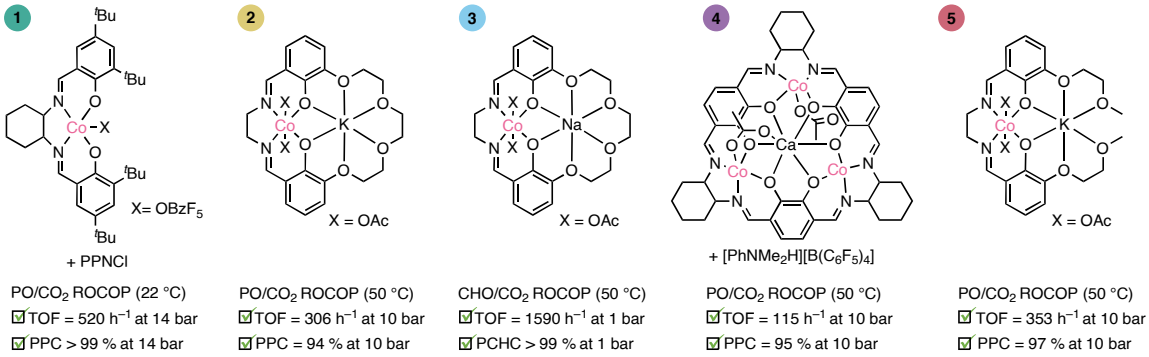

Fig. 2 | Catalysts studied in this work. The structures and key data for the catalysts **1**[33], **2**[34], **3**[34], **4**[41] and **5**[13]. The figure includes turnover frequency (TOF) and selectivity for polycarbonate data at the lowest carbon dioxide pressure reported in the original publications. ᵗBu, tertiary butyl (−C(CH$_3$)$_3$); OBzF$_5$, pentafluorobenzoate (−OCOC$_6$F$_5$); Ph, phenyl (−C$_6$H$_5$); PPNCl, bis(triphenylphosphine)iminium chloride; OAc, acetate (−OCOCH$_3$).

evaluated the literature for catalysts with precedent for good activity (turnover frequency >100 h^{-1}) and selectivity (>90%) at low CO$_2$ pressures (≤10 bar) (Supplementary Fig. 1 and Supplementary Table 2). We also selected catalysts that retain their performances at medium to high temperatures (45–100 °C), so as to maximize rates while minimizing polymer viscosity[29]. From a long list of catalysts showing optimum performances at pressures below 30 bar, catalysts **1**–**4** were selected[13,33,34,41]. They fulfil the performance criteria, are synthetically accessible and represent different classes including both mono-metallic or multi-metallic catalysts and catalysts operating with or without cocatalysts (Fig. 2). The rates for each of these catalysts were determined under varied CO$_2$ pressures (2–30 bar) and using otherwise identical conditions[33,34,41]. The results of these experiments are compared to the previously reported Co(III)K(I) catalyst **5** for which the CO$_2$ insertion equilibrium was proposed[13] (Fig. 2).

All these leading catalysts are cobalt complexes, as it outperforms other metal choices[21,33,35,42] (Supplementary Table 2). Since the leading commercial epoxide is PO, PO–CO$_2$ ROCOP catalysts were investigated first[9,35]. However, the copolymerization of CHO (CHO–CO$_2$ ROCOP) is also a commonly used catalyst benchmark in the field, hence catalyst **3** was investigated for CHO–CO$_2$ ROCOP[34].

Kinetics

Catalysts **1**–**5** were prepared according to literature procedures[13,33,34,41], characterized using infrared and ultraviolet-visible light spectroscopy and, where possible, using ^{1}H and ^{13}C NMR spectroscopy (Supplementary Figs. 2–33).

To investigate whether catalysts **1**–**4** exhibit behaviours consistent with a metal-alkoxide and CO$_2$ insertion equilibrium, kinetic analyses were conducted using each catalyst. All reactions were conducted in neat epoxide since these conditions are desirable at scale (no organic solvents). Catalysts should also control the polycarbonate molar mass, dispersity and polymer chain end-groups, specifically maintaining activity when using excess (di)alcohols, controlling for (di)hydroxyl polymer end-groups[43]. All polymerizations were therefore conducted in the presence of *trans*-1,2-cyclohexanediol in neat epoxide, that is [catalyst]:[diol]:[epoxide] = 1:20:4,000 at 50 °C.

Taking catalyst **2** as a representative example of the experiments conducted for each of the catalysts, first, a series of polymerizations were conducted under CO$_2$ pressures from 2 bar to 25 bar. At a fixed pressure, polymerizations were monitored using in situ infrared spectroscopy allowing for the calculation of a pseudo first-order rate constant, k_{obs}, from the semi-logarithmic plot of ln([epoxide]/[epoxide]$_0$) versus time (Fig. 3b,c). Experiments were conducted at least in duplicate to enable quantification of errors. Next the k_{obs} values were plotted against the applied CO$_2$ pressures, showing a linear increase in rate from 2–14 bar (Fig. 3d). The same data plotted as ln(k_{obs}) versus ln(P(CO$_2$)) have a gradient of 0.97, indicating a first-order rate dependence on CO$_2$ pressure (Fig. 3e). At pressures above 14 bar CO$_2$, the rates were constant and no further increase in k_{obs} was observed. Above the threshold pressure (14 bar), $P_{threshold}$, there is a zero-order dependence on CO$_2$ pressure (Fig. 3d). Polymerization rates were also plotted against [CO$_2$], showing the same trends[13,44] (Supplementary Figs. 43–46).

The experimental kinetic data for all the catalysts were collected and analysed in the same way as for catalyst **2**. All catalysts showed two different regimes of activity versus CO$_2$ pressure, and for each catalyst a threshold pressure was identified as the lowest operating pressure for maximum rates (Supplementary Figs. 43–46). These kinetic data indicate that catalysts **1**–**4** all show metal-alkoxide and CO$_2$ insertion equilibria (Fig. 1b). These data are interpreted by low pressures resulting in CO$_2$ insertion equilibria controlling the effective concentration of the carbonate intermediate, which is the key intermediate in the catalytic rate-determining step. Above the threshold CO$_2$ pressure, the equilibrium lies towards the carbonate and maximum rates result[13].

The CO$_2$ insertion equilibrium constant was determined for all five catalysts in the same way. In brief, in the CO$_2$ pressure independent regime, the equilibrium lies entirely towards the carbonate intermediate, hence [catalyst]$_0$ = [carbonate], assuming the catalyst can only be speciated as an alkoxide or carbonate intermediate (that is, no catalyst decomposition occurs). The carbonate intermediate concentration at a given pressure, [carbonate]$_p$, was determined from the ratio of the rate constant at that pressure and the maximum rate constant, multiplied by maximum carbonate concentration. Accordingly, the CO$_2$ insertion equilibrium constant, K_{eq}, was determined at each pressure and an average value determined (Supplementary Tables 7–12).

$$K_{eq} = \frac{[\text{carbonate}]}{[\text{alkoxide}][CO_2]} \quad (1)$$

The five catalysts show K_{eq} values that vary from 0.25 ± 0.02 M^{-1} for catalyst **4** to 3.10 ± 0.26 M^{-1} for catalyst **3** (Supplementary Tables 7–12). A common rate law was proposed that accounts for the influence of the CO$_2$ insertion equilibrium and the concentration of the metal-alkoxide intermediate: this rate law applies at all CO$_2$ pressures (equation 2). Next, for each catalyst the experimental conversion versus time data was compared to data modelled using the rate law (Fig. 3f for catalyst **2** and Supplementary Fig. 34). All catalysts showed an excellent agreement between the experimental and kinetic model data over the entire data range. This finding, applicable to all five catalysts, underscores the generality of the rate law and utility of quantifying the CO$_2$ insertion equilibria (K_{eq}).

$$\text{Rate} = k_p K_{eq} [\text{alkoxide}] [CO_2] [\text{epoxide}] \quad (2)$$

https://doi.org/10.1038/s41557-026-02098-6

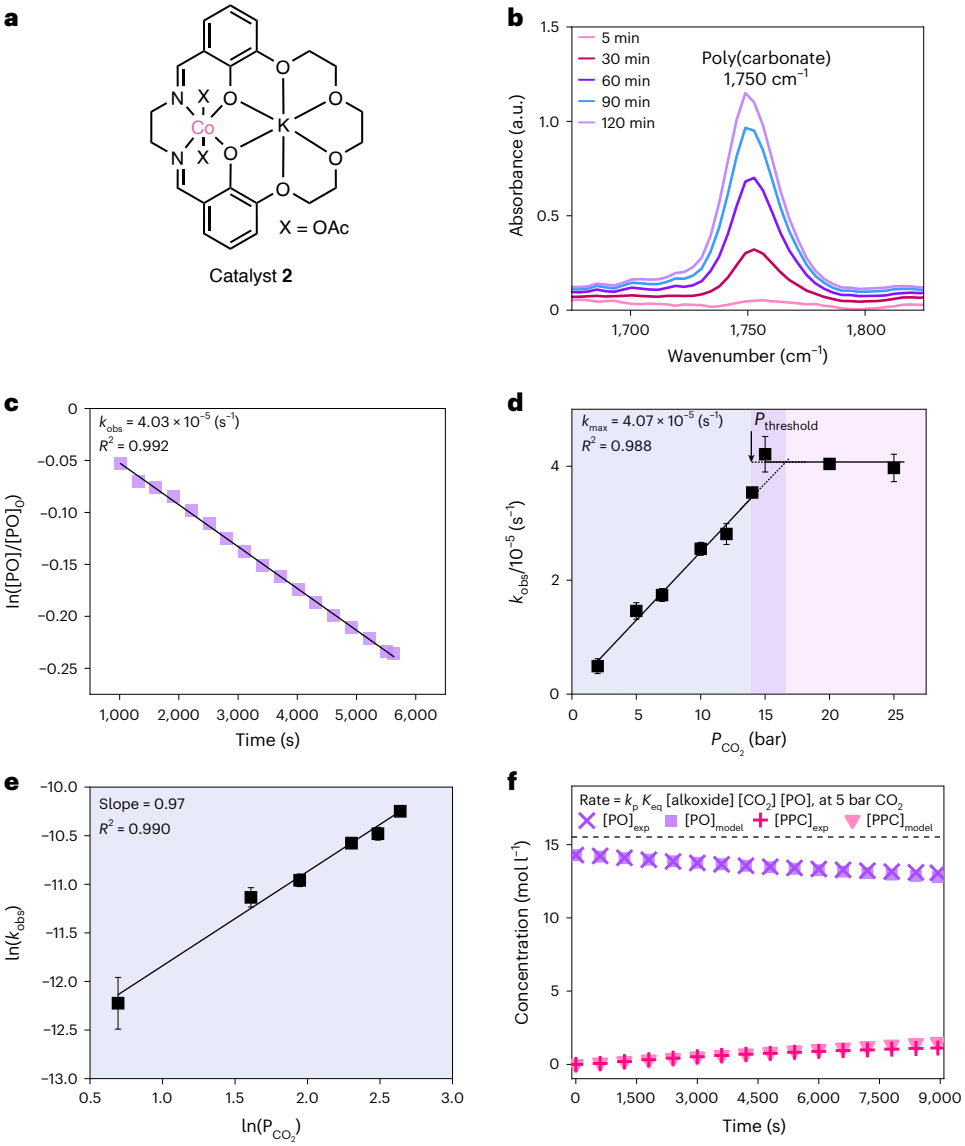

Fig. 3 | Kinetic analysis conducted using catalyst 2. a, Structure of catalyst **2**. **b**, In situ infrared spectrum, showing the peaks corresponding to PPC (1,750 cm^{-1}). **c**, Exemplar semi-logarithmic plot of $[PO]/[PO]_0$ versus time, where the rate constant, k_{obs}, is the slope of the graph, using the rate data for the polymerization at 25 bar CO_2. It has previously been shown that values for such initial rates compare very well with integrated rates determined over wider conversion ranges (20–80%)[51]. **d**, Experimentally determined rates (k_{obs}) versus $P(CO_2)$. All rate constants were determined as the average of $n = 2$ independent runs, with errors indicated as ± the standard error from the mean, typically falling ±10%. k_{max} is the maximum polymerization rate constant, determined as the mean of the k_{obs} values in the CO_2 pressure independent regime. **e**, Plot of $\ln(k_{obs})$ versus $\ln(P(CO_2))$ showing a gradient of 0.97. All $\ln(k_{obs})$ values were determined from k_{obs} values obtained as the average of $n = 2$ independent runs, with errors indicated as ± the standard error from the mean. **f**, Concentration versus time plot showing the excellent agreement between the experimental data and data generated using the rate law and modelled using COPASI software (Supplementary Fig. 34 and Supplementary Tables 3–6).

Variable substrate concentration-rate dependencies, observed with CO_2 pressure in this work, are also known in other fields, for example enzyme kinetics[45]. The data for catalyst **2** were also fit using a Michaelis–Menten kinetic model. Plotting the initial rate, υ_i, against $[CO_2]$, and fitting with the Michaelis–Menten model, revealed $K_{eq} = 0.49\ M^{-1}$ and $\upsilon_{max} = 6.6 \times 10^{-4}\ Ms^{-1}$, which are in good agreement with the values for $K_{eq} = 0.62 \pm 0.09\ M^{-1}$ and $\upsilon_{max} = 5.8 \times 10^{-4}\ Ms^{-1}$ determined using the rate law presented in this work (Supplementary Fig. 52). The benefit of using our experimental and kinetic methods are that they directly determine the carbon dioxide insertion equilibrium constant K_{eq} and the threshold CO_2 pressure $P_{threshold}$, the latter is absent from saturation kinetic models.

Generality of metal alkoxide and CO_2 insertion equilibrium

According to the common rate law, the CO_2 insertion equilibrium constant directly correlates with the polymerization rate. Therefore, we plotted the CO_2 insertion equilibrium constant, K_{eq}, for each of catalysts **1**–**5**, against their rates, measured at 5 bar CO_2 and 50 °C ($k_{obs,5\ bar}$). The plot reveals a clear exponential correlation between carbon dioxide insertion equilibrium constant and rate (Fig. 4b and Supplementary Fig. 53). The highest performing catalyst (**3**) exhibits the highest CO_2 insertion equilibrium constant, 3.10 ± 0.26 M^{-1}. Conversely, the lowest performing catalyst (**4**) has the lowest CO_2 insertion equilibrium constant, 0.25 ± 0.02 M^{-1} (Fig. 4b–d).

These activity correlations underline the importance of CO_2 insertion equilibria across the different catalysts and provide a new way to compare and design better catalysts. To interpret the data, a mechanism whereby the rate-determining step involves catalyst carbonate attack on the epoxide is invoked (Fig. 1b). The concentration of this key catalyst species (metal carbonate) is controlled by the CO_2 insertion equilibrium. Thus, catalysts with favourable CO_2 insertion equilibria,

https://doi.org/10.1038/s41557-026-02098-6

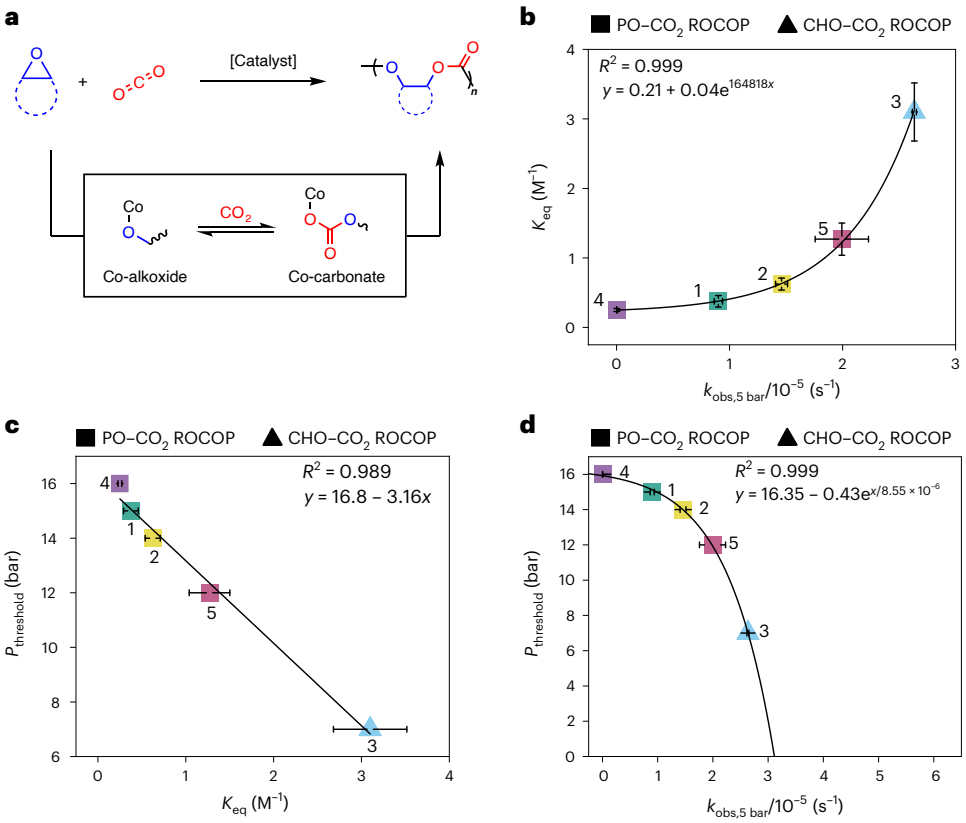

Fig. 4 | Relating the CO_2 insertion equilibrium constant, K_{eq}, to polymerization rates. a, General reaction scheme for epoxide–CO_2 ROCOP showing the proposed CO_2 insertion equilibrium between a Co-alkoxide and a Co-carbonate intermediate. **b**, Plot showing all catalysts and values for K_{eq} versus k_{obs} at 5 bar CO_2 pressure and 50 °C. All k_{obs} values were determined as the average of $n = 2$ independent runs, with errors indicated as ± the standard error from the mean, typically falling ±10%. Values for K_{eq} and corresponding errors were calculated as indicated in Supplementary Tables 7–12. **c**, Plot showing data for all catalysts with $P_{threshold}$ versus K_{eq}. Values for K_{eq} and corresponding errors were calculated as indicated in Supplementary Tables 7–12. **d**, Plot showing data for all catalysts with $P_{threshold}$ versus k_{obs}, at 5 bar CO_2 pressure and 50 °C. All k_{obs} values were determined as the average of $n = 2$ independent runs, with errors indicated as ± the standard error from the mean, typically falling ±10%. In all plots, squares represent PO–CO_2 ROCOP and triangles represent CHO–CO_2 ROCOP. The symbol colours correspond to the catalysts colour with their associated numbering as defined in Fig. 2. Data for catalyst 5 were taken from ref. 13.

for example catalyst **3**, show greater catalytic performance. The slower and less selective catalysts, for example catalysts **1** or **4**, show low CO_2 insertion equilibrium constants, consistent with higher concentrations of residual alkoxide intermediate.

The threshold CO_2 pressure, $P_{threshold}$, values describe the minimum CO_2 pressure to achieve the maximum rate. These values are likely to be very important to any process to make polymers[1,4–6]. The values vary considerably for catalysts **1**–**5** from 7–16 bar CO_2. Plotting, $P_{threshold}$ against K_{eq}, for catalysts **1**–**5** reveals a linear correlation (Fig. 4c). The better performing catalysts have higher equilibrium constants and lower $P_{threshold}$: that is, they reach maximum performance at lower CO_2 pressures. $P_{threshold}$ also exponentially correlates to the measured $k_{obs,5\,bar}$ (Fig. 4d). This kinetic treatment directly links two measurable variables: the rate constant, $k_{obs,5\,bar}$ and $P_{threshold}$, a parameter central to low energy process operation. Such a correlation is particularly important, since it identifies how to maximize performances while minimizing the operating pressure with its associated economic and environmental costs (Supplementary Table 1).

Prediction of equilibrium parameters

There are clear correlations between rate, equilibrium and threshold pressure that apply to all five catalytic systems, which span a wide range of different catalyst classes (Fig. 2). One consequence is that these correlations could be generalizable to other epoxide–CO_2 copolymerizations, conducted isothermally, with experiments in this work all being conducted at 50 °C. It may be that the carbon dioxide insertion K_{eq} and $P_{threshold}$ are predictable for any catalyst or monomer using a single measurement of rate coefficient, k_{obs}, which is set in this work at 5 bar. To experimentally test this hypothesis, a previously reported heterodinuclear Co(II)Mg(II) catalyst (**6**), not included in the original catalyst selection, was synthesized and examined for CHO–CO_2 ROCOP[46] (Supplementary Fig. 54 and Supplementary Table 13). Catalyst **6** was selected as it showed very high performances in the copolymerization catalysis, including operating at low loadings and temperatures. In addition, catalysts **1**, **2** and **5**, previously investigated for PO–CO_2 ROCOP, were each examined for a second monomer combination: CHO–CO_2 ROCOP. First, each catalyst was monitored for CHO–CO_2 ROCOP, at 5 bar CO_2 pressure, to obtain the rate coefficient $k_{obs,5\,bar}$. Using $k_{obs,5\,bar}$, the CO_2 insertion equilibrium constant, K_{eq}, and threshold pressure, $P_{threshold}$, were predicted using the exponential relationships that were previously uncovered (Figs. 4 and 5 and Supplementary Table 13). The predicted equilibrium constants for catalysts **1**, **5** and **6** are comparable, with $K_{eq} = 0.27\ M^{-1}$ (**1**), $0.85\ M^{-1}$ (**5**) and $0.28\ M^{-1}$ (**6**) (Supplementary Table 13). They also show similar, high, values for the predicted $P_{threshold} = 16$ bar (**1** and **6**) and 14 bar (**5**). In contrast, catalyst **2** has a substantially higher predicted CO_2 insertion equilibrium constant, $K_{eq} = 23.4\ M^{-1}$ and a notably lower predicted $P_{threshold}$ (Fig. 5). To further investigate the general predictability of K_{eq}, a previously reported organoborane catalyst was tested for CHO–CO_2 ROCOP[47] (Supplementary Fig. 54 and Supplementary Table 13). However, the observed activities were too low under these conditions to warrant further equilibrium or rate analysis.

https://doi.org/10.1038/s41557-026-02098-6

a

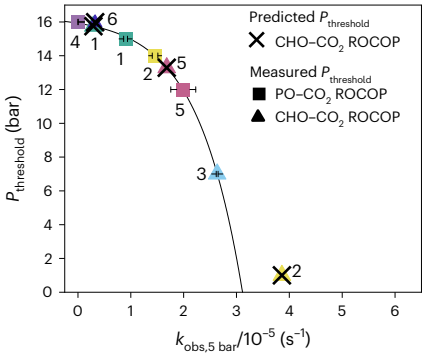

b

Catalyst	Predicted $P_{threshold}$ (bar)	$k_{obs,\ Pthreshold}$ (s^{-1})	$k_{obs,\ 20\ bar}$
1	16	0.85×10^{-5}	0.86×10^{-5}
2	<5	3.86×10^{-5}	3.91×10^{-5}
5	14	3.90×10^{-5}	4.10×10^{-5}
6	16	0.91×10^{-5}	0.77×10^{-5}

c

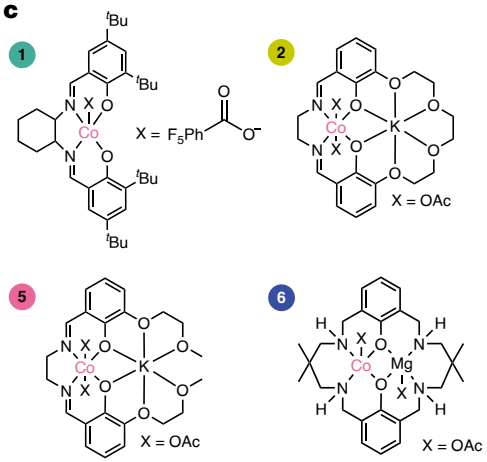

Fig. 5 | Prediction of threshold pressures for maximum catalytic performance. **a**, Plot of threshold pressure for maximum catalytic performance ($P_{threshold}$) versus polymerization rate constant, k_{obs}, at 5 bar CO_2 pressure and 50 °C. Squares represent k_{obs} for the PO–CO_2 ROCOP, and triangles for CHO–CO_2 ROCOP. k_{obs} values were determined as the average of $n = 2$ independent runs, with errors indicated as ± the standard error from the mean, typically falling ±10%. Data for catalyst 5 were taken from ref. 13. Crosses represent measured values of $k_{obs,5\ bar}$ and predicted $P_{threshold}$ values for catalysts **1**, **2**, **5** and **6** for the CHO–CO_2 ROCOP (Supplementary Table 13). **b**, Table showing the predicted $P_{threshold}$ and the measured catalytic performance at $P_{threshold}$ and at a pressure above it (20 bar) for catalysts **1**, **2**, **5** and **6**. The rate data, k_{obs}, were obtained at 50 °C, using catalyst (0.025 mol%, 2.5 mM), CHO (6 ml, 9.9 M), *trans*-1,2-cyclohexanediol (0.5 mol%, 49 mM). **c**, Structures of the catalysts **1**, **2**, **5** and **6** for which $P_{threshold}$ was successfully predicted. The symbol colours in the graphs correspond to the catalysts colour with their associated numbering as defined in Fig. 2.

Following the predictions of $P_{threshold}$ and K_{eq}, the accuracy of the predicted values for catalysts **1**, **2**, **5** and **6** was tested experimentally. For catalyst **5**, CHO–CO_2 ROCOP was investigated at pressures from 5 bar to 25 bar, with the $P_{threshold}$ being 14 bar and matching the predicted value (Supplementary Fig. 55). For catalyst **1** and **6**, the value of the predicted pressure threshold is tested by conducting CHO–CO_2 ROCOP at the predicted $P_{threshold}$ (16 bar CO_2, Fig. 5), and at a higher pressure than the threshold (20 bar CO_2). If the predicted $P_{threshold}$ is accurate, the catalytic performance should remain unchanged and indeed, the k_{obs} is equivalent at each of those pressures ($k_{obs,16\ bar} = 0.85 \times 10^{-5}\ s^{-1}$, $k_{obs,20\ bar} = 0.86 \times 10^{-5}\ s^{-1}$ for catalyst **1** and $k_{obs,16\ bar} = 0.91 \times 10^{-5}\ s^{-1}$, $k_{obs,20\ bar} = 0.77 \times 10^{-5}\ s^{-1}$ for catalyst **6**). Catalyst **5** was applied at pressures of 14 (predicted threshold pressure) and 20 bar; it showed very similar rates at both pressures ($k_{obs,14\ bar} = 3.90 \times 10^{-5}\ s^{-1}$, $k_{obs,20\ bar} = 4.10 \times 10^{-5}\ s^{-1}$) once again validating the successful identification of the threshold pressure.

Since catalyst **2** performs far better at 5 bar than the other two catalysts, its $P_{threshold}$ was predicted to be below 5 bar. This result implies that catalyst **2** has already achieved its maximum rates at 5 bar. Hence, catalyst **2** showed the same catalytic performance at both 5 bar and 20 bar ($k_{obs,5\ bar} = 3.86 \times 10^{-5}\ s^{-1}$, $k_{obs,20\ bar} = 3.91 \times 10^{-5}\ s^{-1}$), strongly suggesting that its $P_{threshold}$ is <5 bar (Fig. 5 and Supplementary Table 13). These experiments are surprising since the data generated using PO–CO_2 ROCOP can be used to successfully predict $P_{threshold}$ for CHO–CO_2 ROCOP and to accelerate identification of the optimum operating conditions, that is, minimum pressure for maximum rate. The results obtained using catalysts **1**, **2**, **5** and **6** for the CHO–CO_2 ROCOP indicate that the kinetic methods may be further generalizable to other monomers. It is particularly helpful to use a single kinetic evaluation ($k_{obs,5\ bar}$) to identify and predict the optimum operating conditions for that catalyst.

The general applicability of K_{eq} as a predictor of catalytic performance is further illustrated by three other known catalysts for which pressure-dependent kinetics were reported[26,27,48]. An antimony catalyst (with bis(triphenylphosphine)iminium chloride co-catalyst) showed an equilibrium constant of <1 bar^{-1} in CHO–CO_2 ROCOP, resulting in a $P_{threshold}$ > 20 bar (Supplementary Fig. 56). A similar $P_{threshold}$ above 20 bar was reported for a di-Zn(II) β-diiminate catalyst. By contrast, a zinc β-diiminate catalyst **7** showed a threshold pressure <5 bar CO_2 pressure[26]. In the original reports no equilibrium constants were determined; however, we estimated K_{eq} <1 M^{-1} and K_{eq} ~ 3.67 M^{-1} for the zinc catalysts, respectively (Fig. 6, catalyst **7**).

The kinetic prediction method indicates that only catalysts with $k_{obs,5\ bar} > 2.5 \times 10^{-5}\ s^{-1}$ ($K_{eq} > 10\ M^{-1}$), are expected to show CO_2 pressure independent performances below 10 bar. The PO–CO_2 ROCOP catalysts examined all show $K_{eq} < 5\ M^{-1}$, and at 5 bar all show performances that depend on carbon dioxide pressure (squares, Fig. 6). Even in the broader literature there are not yet any PO–CO_2 ROCOP catalysts known or reported to enter the target regime: that is, showing high rates and selectivity at <10 bar pressure. The methods presented here should help accelerate new catalyst testing and identify catalyst structure–performance relationships, particularly focused on how catalyst structure drives carbon dioxide insertion chemistry. In contrast, for CHO–CO_2 ROCOP, catalyst **2** already shows a $K_{eq} > 10\ M^{-1}$ and achieves excellent performances at <5 bar CO_2 pressure (Fig. 6). The literature also reveals other CHO–CO_2 ROCOP catalysts reported to exhibit high rates at low CO_2 pressures; these catalysts are recommended for evaluation using the methods reported here to confirm whether pressure independent performances are achieved at <10 bar. Where such criteria are achieved, the catalysts may even function using more dilute CO_2 sources (that is, <1 bar pressure): a regime that is very rarely explored in this field of catalysis[46,49].

Both catalyst structure and monomer choice influence the CO_2 insertion chemistry, highlighting the value in using the CO_2 insertion parameters, K_{eq} and $P_{threshold}$, as metrics for catalyst comparison. One benefit of these metrics is that they inform directly on the process operating conditions with respect to catalytic performance. Comparing catalysts using these parameters may be more informative than the conventional use of activity (that is, turnover frequency) as figure of merit. It is well known that such activity measurements are both monomer and condition dependent; in contrast, K_{eq} allows for comparisons over a range of CO_2 pressures and different epoxides. The ability to rapidly predict the carbon dioxide insertion K_{eq} or $P_{threshold}$ values drastically reduce the experimental work needed to compare new catalysts and to identify the lowest pressure operating conditions for them.

The correlations and the practical experimental protocols should be especially useful in selecting catalysts for larger-scale use, and in

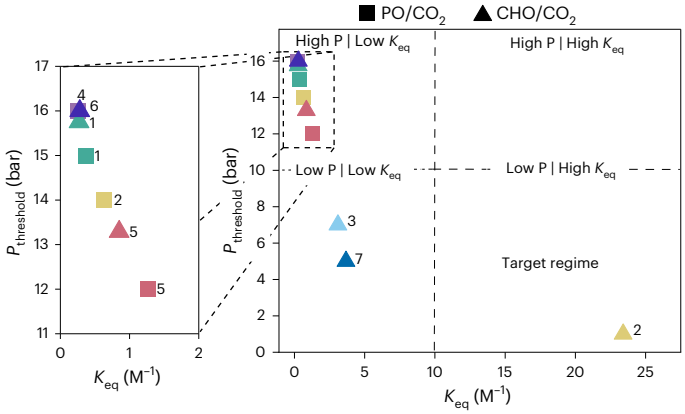

Fig. 6 | Relating the value of CO_2 insertion equilibrium constants to threshold pressures for maximum catalytic performance. Plot of the combined data for all catalysts showing the carbon dioxide threshold pressure values, $P_{threshold}$, and CO_2 insertion equilibrium constants, K_{eq}, determined in this investigation (with colours identifying different catalysts and square markers referring to PO–CO_2 ROCOP, triangles to CHO–CO_2 ROCOP). The plot shows that only catalyst **2** applied for CHO–CO_2 ROCOP achieves the target low pressure (<10 bar) and high insertion equilibrium (>10 M^{-1}) performance.

identification of their optimum operating conditions[50]. One question raised by this work is the extent to which similar CO_2 insertion equilibria, and threshold pressures, may apply to other CO_2 utilization catalyses? The use of the methods outlined in this report is recommended to explore CO_2 insertion equilibria in other catalytic cycles. The methods may be particularly useful in identifying operable, fast and selective catalysts that are needed to implement large-scale, energy efficient CO_2 uses.

Conclusions

The influence of CO_2 pressure on its insertion reactions into metal-alkoxide bonds was investigated using structurally diverse, high-performance epoxide and carbon dioxide ROCOP catalysts. Systematic experiments, conducted using epoxide and CO_2 at pressures from 2 bar to 30 bar, revealed that all five catalysts show pressure-dependent CO_2 insertion equilibria. A rate law, applicable under all pressures, was presented and interpreted by a mechanism accounting for differing extents of carbon dioxide insertion. Two reaction parameters are identified and methods to quantify them are presented: the CO_2 insertion equilibrium constant (K_{eq}) and the threshold carbon dioxide pressure above which rates are maximized ($P_{threshold}$). Direct correlations were uncovered between catalytic rate and the CO_2 insertion equilibrium constant and threshold pressure. The data, and parameter inter-relationships, were used to successfully predict the performances for known catalysts using new monomers (CHO–CO_2). The use of one measurement, rather than full kinetic analyses, substantially reduces the experimental work required to identify the lowest pressure process operating conditions and provides a reliable set of metrics by which to compare catalysts. The findings are particularly important for future catalyst design, specifically the under-recognized importance of design for CO_2 insertion, and in enabling scale-up of catalysts resulting in the lowest energy demand. Given the importance of CO_2 insertion equilibria in influencing this field of carbon dioxide copolymerization catalysis, it seems possible, if not likely, that other catalysts may also show related CO_2 pressure dependence. Identifying and quantifying the lowest energy conditions for such CO_2 insertions is really important to accelerate delivery of large-scale CO_2 utilization processes and products.

Online content

Any methods, additional references, Nature Portfolio reporting summaries, source data, extended data, supplementary information, acknowledgements, peer review information; details of author contributions and competing interests; and statements of data and code availability are available at https://doi.org/10.1038/s41557-026-02098-6.

References

1. Vidal, F. et al. Designing a circular carbon and plastics economy for a sustainable future. *Nature* **626**, 45–57 (2024).
2. Carus, M., Dammer, L., Raschka, A. & Skoczinski, P. Renewable carbon: key to a sustainable and future-oriented chemical and plastic industry: definition, strategy, measures and potential. *Greenhouse Gases Sci. Technol.* **10**, 488–505 (2020).
3. Bachmann, M. et al. Towards circular plastics within planetary boundaries. *Nat. Sustain.* **6**, 599–610 (2023).
4. Hepburn, C. et al. The technological and economic prospects for CO_2 utilization and removal. *Nature* **575**, 87–97 (2019).
5. Klos, N. et al. Concatenating microbial, enzymatic, and organometallic catalysis for integrated conversion of renewable carbon sources. *JACS Au* **4**, 4546–4570 (2024).
6. Burger, J. et al. Environmental impacts of carbon capture, transport, and storage supply chains: status and the way forward. *Int. J. Greenhouse Gas Control* **132**, 104039 (2024).
7. Nakano, R., Ito, S. & Nozaki, K. Copolymerization of carbon dioxide and butadiene via a lactone intermediate. *Nat. Chem.* **6**, 325–331 (2014).
8. Liu, Q., Wu, L., Jackstell, R. & Beller, M. Using carbon dioxide as a building block in organic synthesis. *Nat. Commun.* **6**, 5933 (2015).
9. Yang, G.-W., Xie, R., Zhang, Y.-Y., Xu, C.-K. & Wu, G.-P. Evolution of copolymers of epoxides and CO_2: catalysts, monomers, architectures, and applications. *Chem. Rev.* **124**, 12305–12380 (2024).
10. Wu, J. et al. Catalytic conversion of carbon dioxide to propylene carbonate: catalyst design and industrialization progress. *ACS Catal.* **15**, 1305–1340 (2025).
11. Tundo, P., Musolino, M. & Aricò, F. The reactions of dimethyl carbonate and its derivatives. *Green Chem.* **20**, 28–85 (2018).
12. Bierbaumer, S. et al. Enzymatic conversion of CO_2: from natural to artificial utilization. *Chem. Rev.* **123**, 5702–5754 (2023).
13. Eisenhardt, K. H. S., Fiorentini, F., Lindeboom, W. & Williams, C. K. Quantifying CO_2 insertion equilibria for low-pressure propene oxide and carbon dioxide ring opening copolymerization catalysts. *J. Am. Chem. Soc.* **146**, 10451–10464 (2024).
14. Deacy, A. C., Phanopoulos, A., Lindeboom, W., Buchard, A. & Williams, C. K. Insights into the mechanism of carbon dioxide and propylene oxide ring-opening copolymerization using a Co(III)/K(I) heterodinuclear catalyst. *J. Am. Chem. Soc.* **144**, 17929–17938 (2022).
15. Hazari, N. Kinetic studies of CO_2 insertion into metal–element σ-bonds. *Acc. Chem. Res.* **57**, 2847–2858 (2024).
16. Simpson, R. D. & Bergman, R. G. A dramatic difference in the reactivities of alkoxido- and aryloxidorhenium complexes in insertion reactions. *Angew. Chem. Int. Ed.* **31**, 220–223 (1992).
17. Offermans, W. K., Bizzarri, C., Leitner, W. & Müller, T. E. Surprisingly facile CO_2 insertion into cobalt alkoxide bonds: a theoretical investigation. *Beilstein J. Org. Chem.* **11**, 1340–1351 (2015).
18. Phipps, C. A. et al. Metal–ligand cooperativity promotes reversible capture of dilute CO_2 as a Zn(II)-methylcarbonate. *Inorg. Chem.* **62**, 2751–2759 (2023).
19. Phipps, C. A. et al. Enhancing CO_2 capture via metal–ligand cooperativity: tuning ligand basicity and Zn(II) Lewis acidity. *Inorg. Chem.* **63**, 9992–10000 (2024).
20. Liu, Y. & Lu, X.-B. Current challenges and perspectives in CO_2-based polymers. *Macromolecules* **56**, 1759–1777 (2023).
21. Trott, G., Saini, P. K. & Williams, C. K. Catalysts for CO_2/epoxide ring-opening copolymerization. *Philos. Trans. A. Math. Phys. Eng. Sci.* **374**, 20150085 (2016).

22. Ren, W.-M., Liu, Z.-W., Wen, Y.-Q., Zhang, R. & Lu, X.-B. Mechanistic aspects of the copolymerization of CO_2 with epoxides using a thermally stable single-site cobalt(III) catalyst. *J. Am. Chem. Soc.* **131**, 11509–11518 (2009).
23. Liu, J., Ren, W.-M., Liu, Y. & Lu, X.-B. Kinetic study on the coupling of CO_2 and epoxides catalyzed by Co(III) complex with an inter- or intramolecular nucleophilic cocatalyst. *Macromolecules* **46**, 1343–1349 (2013).
24. Ohkawara, T., Suzuki, K., Nakano, K., Mori, S. & Nozaki, K. Facile estimation of catalytic activity and selectivities in copolymerization of propylene oxide with carbon dioxide mediated by metal complexes with planar tetradentate ligand. *J. Am. Chem. Soc.* **136**, 10728–10735 (2014).
25. Cao, H. et al. On-demand transformation of carbon dioxide into polymers enabled by a comb-shaped metallic oligomer catalyst. *ACS Catal.* **12**, 481–490 (2022).
26. Kernbichl, S., Reiter, M., Mock, J. & Rieger, B. Terpolymerization of β-butyrolactone, epoxides, and CO_2: chemoselective CO_2-switch and its impact on kinetics and material properties. *Macromolecules* **52**, 8476–8483 (2019).
27. Lehenmeier, M. W. et al. Flexibly tethered dinuclear zinc complexes: a solution to the entropy problem in CO_2/epoxide copolymerization catalysis?. *Angew. Chem. Int. Ed.* **52**, 9821–9826 (2013).
28. Kemper, G., Hölscher, M. & Leitner, W. Pd(II)-catalyzed carboxylation of aromatic C–H bonds with CO_2. *Sci. Adv.* **9**, eadf2966 (2023).
29. Artz, J. et al. Sustainable conversion of carbon dioxide: an integrated review of catalysis and life cycle assessment. *Chem. Rev.* **118**, 434–504 (2018).
30. Klaus, S., Lehenmeier, M. W., Anderson, C. E. & Rieger, B. Recent advances in CO_2/epoxide copolymerization—new strategies and cooperative mechanisms. *Coord. Chem. Rev.* **255**, 1460–1479 (2011).
31. Jutz, F., Buchard, A., Kember, M. R., Fredriksen, S. B. & Williams, C. K. Mechanistic investigation and reaction kinetics of the low-pressure copolymerization of cyclohexene oxide and carbon dioxide catalyzed by a dizinc complex. *J. Am. Chem. Soc.* **133**, 17395–17405 (2011).
32. Lidston, C. A. L., Severson, S. M., Abel, B. A. & Coates, G. W. Multifunctional catalysts for ring-opening copolymerizations. *ACS Catal.* **12**, 11037–11070 (2022).
33. Cohen, C. T., Chu, T. & Coates, G. W. Cobalt catalysts for the alternating copolymerization of propylene oxide and carbon dioxide: combining high activity and selectivity. *J. Am. Chem. Soc.* **127**, 10869–10878 (2005).
34. Deacy, A. C., Moreby, E., Phanopoulos, A. & Williams, C. K. Co(III)/alkali-metal(I) heterodinuclear catalysts for the ring-opening copolymerization of CO_2 and propylene oxide. *J. Am. Chem. Soc.* **142**, 19150–19160 (2020).
35. Diment, W. T., Lindeboom, W., Fiorentini, F., Deacy, A. C. & Williams, C. K. Synergic heterodinuclear catalysts for the ring-opening copolymerization (ROCOP) of epoxides, carbon dioxide, and anhydrides. *Acc. Chem. Res.* **55**, 1997–2010 (2022).
36. Yang, G.-W. et al. Precision copolymerization of CO_2 and epoxides enabled by organoboron catalysts. *Nat. Synth.* **1**, 892–901 (2022).
37. Yeo, H. et al. Alternatives to fluorinated binders: recyclable copolyester/carbonate electrolytes for high-capacity solid composite cathodes. *Chem. Sci.* **15**, 2371–2379 (2024).
38. Gao, C. et al. High-performance recyclable polyester elastomers through transient strain-stiffening. *Adv. Mater.* **37**, 2416674 (2025).
39. Scharfenberg, M., Hilf, J. & Frey, H. Functional polycarbonates from carbon dioxide and tailored epoxide monomers: degradable materials and their application potential. *Adv. Func. Mater.* **28**, 1704302 (2018).
40. Beharaj, A., McCaslin, E. Z., Blessing, W. A. & Grinstaff, M. W. Sustainable polycarbonate adhesives for dry and aqueous conditions with thermoresponsive properties. *Nat. Commun.* **10**, 5478 (2019).
41. Nagae, H., Matsushiro, S., Okuda, J. & Mashima, K. Cationic tetranuclear macrocyclic $CaCo_3$ complexes as highly active catalysts for alternating copolymerization of propylene oxide and carbon dioxide. *Chem. Sci.* **14**, 8262–8268 (2023).
42. Eisenhardt, K. H. S., Fiorentini, F. & Williams, C. K. Understanding the effect of M(III) choice in heterodinuclear polymerization catalysts. *Inorg. Chem.* **63**, 23438–23449 (2024).
43. Dong, J. et al. Construction of ultralow-molecular-weight CO_2–polyols with self-catalytic performance in polyurethane preparation. *Macromolecules* **57**, 2706–2714 (2024).
44. Foltran, S., Cloutet, E., Cramail, H. & Tassaing, T. In situ FTIR investigation of the solubility and swelling of model epoxides in supercritical CO_2. *J. Supercrit. Fluids* **63**, 52–58 (2012).
45. Choi, B., Rempala, G. A. & Kim, J. K. Beyond the Michaelis–Menten equation: accurate and efficient estimation of enzyme kinetic parameters. *Sci. Rep.* **7**, 17018 (2017).
46. Deacy, A. C., Kilpatrick, A. F. R., Regoutz, A. & Williams, C. K. Understanding metal synergy in heterodinuclear catalysts for the copolymerization of CO_2 and epoxides. *Nat. Chem.* **12**, 372–380 (2020).
47. Yang, G.-W., Zhang, Y.-Y., Xie, R. & Wu, G.-P. Scalable bifunctional organoboron catalysts for copolymerization of CO_2 and epoxides with unprecedented efficiency. *J. Am. Chem. Soc.* **142**, 12245–12255 (2020).
48. Jiang, C. et al. Pnictogen-bonding catalysis: copolymerization of CO_2 and epoxides on antimony(V) platforms. *ACS Catal.* **15**, 17882–17892 (2025).
49. Plajer, A. J. & Williams, C. K. Heterotrimetallic carbon dioxide copolymerization and switchable catalysts: sodium is the key to high activity and unusual selectivity. *Angew. Chem. Int. Ed.* **60**, 13372–13379 (2021).
50. Chapman, A. M., Keyworth, C., Kember, M. R., Lennox, A. J. J. & Williams, C. K. Adding value to power station captured CO_2: tolerant Zn and Mg homogeneous catalysts for polycarbonate polyol production. *ACS Catal.* **5**, 1581–1588 (2015).
51. Trott, G., Garden, J. A. & Williams, C. K. Heterodinuclear zinc and magnesium catalysts for epoxide/CO_2 ring opening copolymerizations. *Chem. Sci.* **10**, 5851–5852 (2019).

Methods

CHO–CO_2 and PO–CO_2 ROCOP procedures and experimental apparatus

The same procedures were followed when conducting the CHO–CO_2 and PO–CO_2 ROCOP. A representative method for the CHO–CO_2 ROCOP is detailed here.

The catalyst (0.015 mmol), *trans*-1,2-cyclohexanediol (35 mg, 0.3 mmol) and mesitylene (21 µL, 0.15 mmol, internal standard for monomer conversion quantification) were dissolved in CHO (6 ml, 59 mmol), under a nitrogen atmosphere. The solution was injected into a 100-ml Parr reactor fitted with an in situ attenuated total reflectance-infrared spectroscopy probe, under a flow of CO_2. The reactor was pressurized to the desired CO_2 pressure and heated to 50 °C. Mass flow controllers were used to ensure fixed and constant CO_2 pressure throughout the reaction. The reaction was monitored by changes to infrared peaks at 1,750 cm^{-1} (polycarbonate) and 1,820 cm^{-1} (cyclic carbonate). The polymerization was stirred continually at the desired temperature and pressure until >30% polycarbonate formation. The reaction was then cooled and quenched by exposure to air and addition of benzoic acid (2 mg, 0.016 mmol). The epoxide conversion data was externally calibrated by ^{1}H NMR spectroscopy using a crude reaction aliquot, using the added mesitylene as the internal standard.

The reaction rate coefficient, k_{obs} was determined as the gradient of plots of ln([epoxide]/[epoxide]$_0$) versus time (Supplementary Figs. 39–42), typical epoxide conversions are 5–20%. For each catalyst, epoxide–CO_2 polymerizations were conducted under the same reaction conditions ([catalyst]:[diol]:[epoxide] = 1:20:4,000). For catalysts **1** and **4**, [catalyst]:[cocatalyst] = 1:1. Polymerizations were conducted at 50 °C at a fixed CO_2 pressure, with values systematically increased from 2 bar to 35 bar CO_2, using the reaction set up outlined above. All reactions were run in duplicate, with generally ±10% error. Using previously reported data for the solubility of CO_2 in PO and CHO[13,44], polymerization rates were plotted against both [CO_2] and CO_2 pressure.

Catalyst syntheses

The catalysts **1**–**5** were synthesized according to literature reports. Detailed synthetic procedures for each of catalysts **1**[33], **2**[34], **3**[34], **4**[41] and **5**[13] are provided in the Supplementary Information.

Data availability

Data files for the information contained in the paper and supporting information are open access available via the Oxford University Research Archive at https://ora.ox.ac.uk/objects/uuid:94ebb3ae-29ab-4daa-b186-c9f28600ce48 and https://doi.org/10.5287/ora-prkzkoyj9. Source data are provided with this paper.

Acknowledgements

The EPSRC (grant nos. EP/S018603/1 and EP/Z532782/1, to C.K.W.), the University of Oxford East Alpha Scholarship in Sustainable Chemistry (to C.K.W. and supporting R.T.) and the OXICFM Centre for Doctoral Training (grant no. EP/S023828/1) (to C.K.W. and supporting K.H.S.E. and M.L.S.) are acknowledged for research funding.

Author contributions

R.T. and K.H.S.E. contributed equally to this work. R.T., K.H.S.E. and M.L.S.: conceptualization; investigation; methodology; writing, original draft and writing, review and editing. C.K.W.: conceptualization; data curation; funding acquisition; methodology; supervision; writing, original draft and writing, review and editing.

Competing interests

C.K.W. is a director of Econic Technologies. The other authors declare no competing interests.

Additional information

Supplementary information The online version contains supplementary material available at https://doi.org/10.1038/s41557-026-02098-6.

Correspondence and requests for materials should be addressed to Charlotte K. Williams.

Peer review information *Nature Chemistry* thanks Xiaoshuang Feng and the other, anonymous, reviewer(s) for their contribution to the peer review of this work.